Ion-beam-induced transformation of diamond

S. Prawer
School of Physics and Microanalytical Research Centre, University of Melbourne, Parkville, Victoria 3052, Australia

R. Kalish
Solid State Institute and Physics Department, Technion-Israel Institute of Technology, Haifa, 32000, Israel
(Received 2 June 1994; revised manuscript received 9 December 1994)

The ion-beam-induced transformation of insulating diamond to a conducting form of carbon is explored by performing measurements of the electrical conductivity of diamond subject to ion damage. A wide range of implantation temperatures (150–690 K) with both Xe (320 keV) and C (100 keV) ions are employed. The dose dependence of the conductivity, $R(D)$, is found to scale with the nuclear energy deposited in the irradiated volume, thus demonstrating that it is the density of collisionally induced defects that governs the electrical conductivity. The data are analyzed in terms of a model that proposes that the passage of an ion through the solid leaves in its wake conducting spheres of varying radii. The average radius of these spheres is found to decrease from about 2.05 nm for irradiation at 150 K with 320-keV Xe ions to zero for implantation at about 815 K. At critical doses D_c, which depend on the implantation temperature and the ion species, these spheres overlap to form a continuous conductive pathway through the irradiated diamond. In some cases this transition is sharp enough to be well accounted for by a simple percolation theory. Below D_c, $R(D)$ displays complicated nonmonotonic behavior, which is explained as being due to the competition of the contribution of different types of defects to the observed electrical conductivity. Remarkable similarities between the conductivity induced in diamond and fused quartz implanted with C ions under identical conditions are reported.

I. INTRODUCTION

Diamond is a metastable form of carbon in which each carbon atom is tetrahedrally sp^3 bonded to its four nearest neighbors. This strong bonding is responsible for the unique physical and chemical properties of diamond.[1] The stable form of carbon at room temperature and pressure is graphite; a layered material in which carbon atoms are sp^2 bonded in hexagonal sheets leaving delocalized π electrons available for conduction. As a result graphite is electrically conducting exhibiting very anisotropic properties, whereas diamond is a wide band-gap semiconductor.

Bridging between these two allotropes of carbon lie a whole variety of carbon materials which include, among others, amorphous sp^2 bonded carbon (such as thermally evaporated carbon), micropolycrystalline sp^2 bonded graphite (such as glassy carbon), and amorphous sp^3 bonded carbon (sometimes loosely referred to as amorphous diamond), which is structurally analogous to amorphous Si and is formed during low-energy C ion deposition.[2]

Ion implantation is a process in which the energy deposited by the slowing down of the implanted ions into the irradiated volume can be gradually increased by controlling the ion dose. For covalently bonded solids high dose ion implantation usually leads to amorphization; however for diamond an additional level of complexity is involved since the bonds broken by ion impact may rearrange to form the more stable sp^2 structure. Indeed it is known that high dose implantation of diamond leads to graphitization of the irradiated volume.[3] The process by which this occurs and the intermediate phases involved in this transition are not yet understood. In addition, certain applications of the ion-beam-modified material have recently come to light. In these, use is made of the ability to control the electrical conductivity and other physical properties of the ion-damaged material. These applications include: the formation of conducting electrodes for electrochemical uses;[4] the formation of n-type layers for p-n junctions[5] and the production of infrared emitting elements in diamond.[6]

In the present work we explore the nature of the ion-beam-induced transition between diamond and graphite by performing measurements of the electrical conductivity of diamond subjected to ion damage using different ion species, doses and implantation temperatures. Emphasis is given to the dose regime in which the diamond lattice is still intact and can be repaired by thermal annealing, and to implantation temperatures at which the most pronounced changes in the electrical conductivity take place. These are particularly important for devising implantation schemes to achieve successful doping of diamond by ion implantation. Furthermore, the results of the present study regarding the stability of diamond under ion impact may have important implications regarding the ion-beam deposition of diamond films.

Ion implantation in diamond has recently been reviewed.[7,8] Thus, only those points essential to the understanding of the present work will be briefly summarized below. The main features of ion-beam-induced damage of diamond has been studied by various techniques, all of which show that diamond, when implanted with ions to sufficiently high doses, undergoes distinct changes. Ruth-

erford backscattering channeling[9] and electron diffraction[3] measurements show that as a result of ion-beam-induced damage, diamond changes from a perfect crystal to some disordered structure; electron paramagnetic resonance (EPR) shows that many bonds are broken;[10] optically, the transparent diamond turns black and new absorption lines appear.[11] Raman scattering shows that as a result of high dose implantation, diamond can either transform into amorphous carbon (sp^2) or into micropolycrystalline graphite, depending on implantation temperature;[12] Chemically, the inert diamond changes to an etchable material and the electrical conductivity changes from highly insulating to highly conducting with a conductivity approaching that of graphite.[13] For low dose implantations, there is some data which suggests that the diamond exhibits p-type conduction for room-temperature implantations, but n-type for implantations at elevated temperatures.[14,15]

There exists a critical dose D_c common to all of the above observations below which it has been shown that thermal annealing can restore the diamond to a form close to its pristine state. However, for $D > D_c$ thermal annealing leads to the conversion of the damaged diamond layer to graphite, as is shown, for example, by the susceptibility of the material to etching in hot acids. This critical dose depends on ion mass and energy in a form which has been shown to scale for a given implantation temperature to the energy deposited in the irradiated volume by the nuclear collision process.[16] However it should be noted that D_c is very dependent on implantation temperature, T_i; indeed for sufficiently high T_i graphitization can be completely avoided.

The most striking manifestation of ion-induced damage in diamond is the change in electrical resistivity R as a function of ion dose, D. The R vs D dependence was studied by Vavilov *et al.*[3] for Ar-implanted diamond and later by Kalish *et al.*[17] for Sb, by Prins[8,13] for C, and by Prawer, Hoffman, and Kalish for C and Xe implantations.[18] The features common to all these studies are that several distinct regions in the behavior of R as a function of dose can be identified. For example, included in Fig. 1 is the R vs D curve for diamond implanted at room temperature with 100 keV C ions, which is typical of the results obtained using other ions for room-temperature implantations. For $D < D_1$ the resistivity decreases, but for $D_1 < D < D_c$ the resistivity increases with increasing ion dose. For $D \simeq D_c$ a sharp drop in R is observed. At higher doses the resistivity saturates at a value comparable to that of polycrystalline graphite, and displays metallic-like conduction.[19] It has been found that D_1 corresponds to an energy deposition per target atom of about 1 eV/ target atom and D_c to a value of about 5 eV/target

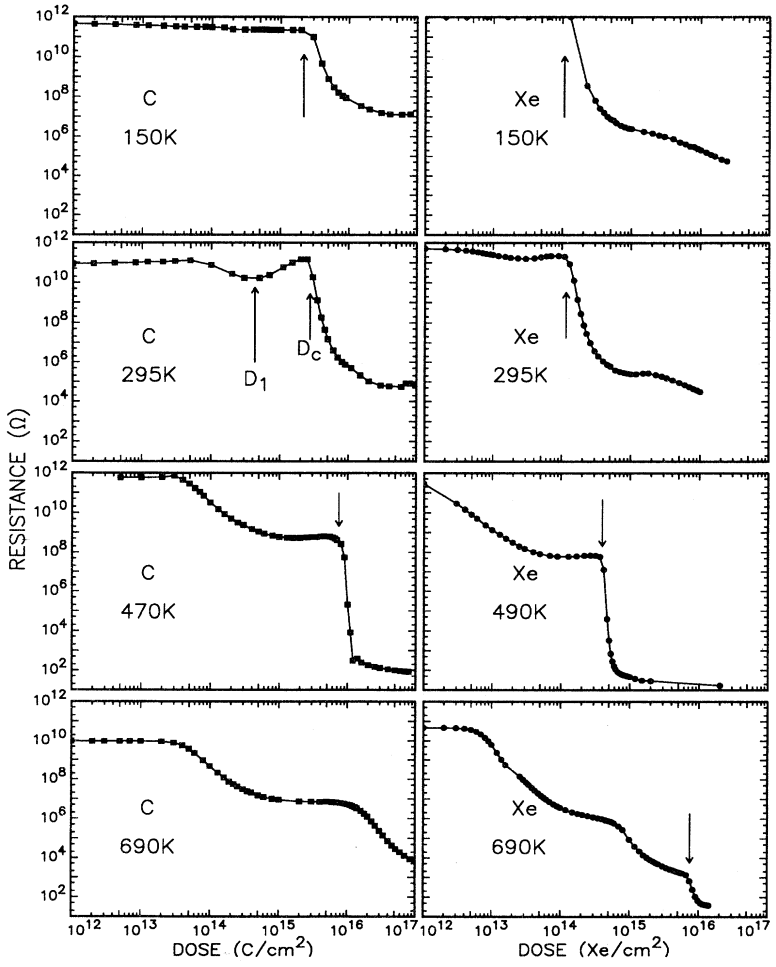

FIG. 1. Resistance of diamond as a function of dose for 100 keV C and 320 keV Xe implantations. The implantation temperature is indicated in the figure. The arrows identify the doses at which overlap between conducting zones occurs (see text). For the implantation with 100 keV C at 295 K, in addition to the critical dose D_c, a minimum in the R vs D curve occurs for a dose D_1, which is also observed for implantation with 320 keV Xe.

atom[16] for a wide variety of room-temperature implantation conditions. The above values of D_1 and D_c are only valid for room-temperature implantations and change with implantation temperature (T_i).

Of the above features in the dose dependence of the resistivity, the value of saturation resistivity (R_s) at high ion doses has been the most studied. It was found[8,12,13] that the implantation temperature T_i strongly affects R_s. R_s exhibits a maximum for liquid-nitrogen implantations, but drops sharply by up to five orders of magnitude around room temperature and reaches a minimum at $T_i \simeq 500$ K.[8] For very hot implantations ($T_i \simeq 1200$ K), R_s rises again to values comparable to those of nonimplanted diamond. Another feature of the final state of heavily implanted diamond is a pronounced swelling of the implanted region.[20] This phenomenon, too, displays a sharp dependence on implantation temperature, decreasing linearly with increasing T_i until at $T_i > 700$ K no further swelling is observable.[21] Many of the above observations have been explained by Prins[8] to be due to the different mobilities of vacancies and interstitials in diamond, with interstitials starting to diffuse at about 300 K while vacancies only become mobile at about 800 K.

The dose regime in the vicinity of D_c in which R changes rapidly as a function of dose has also been studied. For $T_i \simeq 300$ K the conductivity in this dose regime is hopping in nature.[7] Kalish *et al.*[17] investigated the possibility that the sharp drop in the resistivity could be explained in terms of a percolation transition between conducting islands produced by the impinging ions, but found that the R vs D dependence for $T_i \simeq 300$ K was not sharp enough to be consistent with such a simple percolation model. Instead, a model involving the gradual amorphization of the implanted region as a whole was proposed. By contrast, recent work using electron spectroscopies on 1 keV Ar irradiated diamond[16] and other recent channeling, swelling, and electrical conductivity data[15] has suggested that the amorphization is a very sudden process and that at D_c the diamond collapses to an amorphous, but still highly insulating form similar in its properties to amorphous diamond. The conclusion which can be drawn from this previous work is that only at doses exceeding those required for amorphization does the *a*-sp^3 structure transform to an *a*-sp^2 state which is electrically conducting.

Hence, while progress has been made in understanding the ion-beam-induced transformation of insulating diamond to some conductive form of carbon due to ion-induced damage, much remains to be elucidated. In the present work, we address the transformation of diamond under the influence of an ion beam by measuring the ion-beam-induced changes in the electrical conductivity. We cover the entire dose range in which changes in R occur, extending the range previously investigated to include both low and very high doses and examining different implantation temperature regimes in which different defects are expected to be mobile. By performing R vs D measurements at various implantation temperatures for both light (C) and heavy (Xe) implants, and by supplementing them by measurements of the temperature dependence of the resistivity (R vs T) insight into the ion-beam-induced transformation is gained.

II. EXPERIMENTAL DETAILS

Type IIa diamonds of dimension $3\times3\times0.25$ mm^3 (sourced from Drukker Corporation) were used in the present experiments. Two Molybdenum strip contacts of approximate dimensions 1×2 mm^2 and of thickness 300 nm were *e*-beam evaporated onto the diamond at 200 °C, leaving a gap of about 1 mm. The contacts thus obtained were Ohmic over the range of voltages used in the measurements. Pressure metal contacts were applied to the Mo pads. The assembly was mounted on a variable temperature target holder using thermally conducting grease to ensure good thermal contact. The sample temperature was monitored by a thermocouple.

A triple aperture system as described elsewhere[22] was employed to monitor the ion current, thus avoiding the interference of the various electrical leads connected to the sample in the determination of the ion dose. The ion beam homogeneously irradiated the gap between the contacts as well as the contacts themselves, using current densities below 2 μA/cm^2 in order to minimize beam heating effects. A Keithley 619 Electrometer capable of measuring resistances up to 2×10^{12} Ω was used. All electrical measurements were performed *in situ* in the implantation chamber at the temperature of the implantation. In most cases the upper bound on the resistance measurements prior to implantation was limited instrumentally, although for some measurements, surface contamination sometimes resulted in a preimplantation resistance of about 1×10^{11} Ω. For implantations performed at 690 K, the upper bound was due to leakage through the diamond itself which was about 1×10^{10} Ω.

Implantation of C at 100 keV ($R_p \pm \Delta R_p = 130+22$ nm) and Xe at 320 keV ($R_p \pm \Delta R_p = 56\pm9$ nm), where R_p and ΔR_p are the range and straggling, respectively, of the incident ion[23] were performed at 150, 295, 490, and 690 K. Following each implantation dose a stabilization time of about 5 min was allowed before taking the resistance measurement. In order to determine the mechanism of electrical conduction post implantation R vs T measurements were performed in vacuum covering the temperature range 100–300 K for some selected samples.

III. RESULTS

The resistance versus dose for the Xe and C implantations performed at the specified temperatures are shown in Fig. 1. The similarity in the functional dependence for Xe and C implants for the same temperature should be noted.

Figure 2 shows the R vs T data for diamond implanted at 150 K with 8×10^{16} C/cm^2 plotted as $\log(R)$ vs $(1/T)^{1/4}$. The data when plotted in this way exhibit a linear dependence (with a correlation coefficient from a linear least-squares fit to the data of 0.998) indicating that the conduction mechanism follows the variable-range-hopping formula[24]

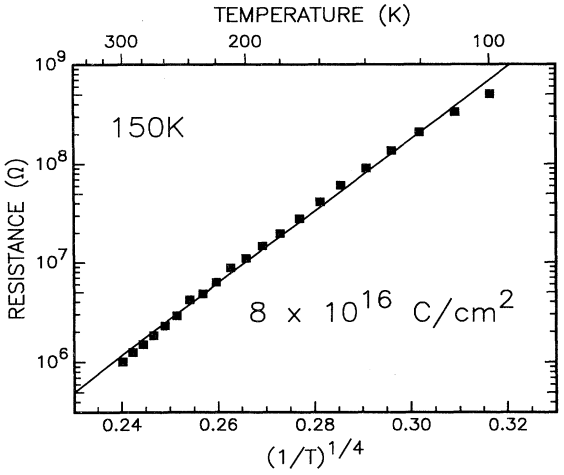

FIG. 2. Resistance versus temperature plotted as R vs $T^{-1/4}$ for diamond irradiated at 150 K with 8×10^{16} C/cm^2 at 100 keV.

$$R(T)=R_0\exp(T_0/T)^{1/4}, \quad (1)$$

where $T_0=16\lambda^{-3}/k_BN(E_F)$, k_B is Boltzmann's constant, λ is the radius of the localized wave function, and $N(E_F)$ is the density of states at the Fermi level.[24] The same data when plotted as $\log(R)$ vs $(1/T)$ do not follow a linear dependence. Similar behavior is observed for a sample irradiated with 2×10^{16} Xe/cm^2 at 150 K. From the slope of the least-squares straight line fit to the data shown in Fig. 2 the value of $T_0(\mathrm{C})=(5\pm0.3)\times10^7$ K. For the Xe-irradiated sample, $T_0(\mathrm{Xe})=(1.4\pm0.1)\times10^6$ K.

Clearly, a measurement of T_0 alone is not sufficient to determine both $N(E_F)$ and λ. In the discussion that follows it will be shown that λ may be determined from an analysis of the R vs D data and hence the above values of T_0 may be used to estimate the density of states at the Fermi level for the implanted diamond.

IV. DISCUSSION

In the present work the ion species used were deliberately chosen so as to exclude doping effects on the observed conductivity; Xe being a large heavy inert gas atom and C being nonalien to the diamond matrix. It should be borne in mind, however, that it has been shown[25] that heavy dose implantation of carbon into insulating matrices such as SiO_2 eventually gives rise to electrical conductivity due to formation of a heavily doped C layer.

Since the dominant effect that must be considered to account for the present data is ion-beam-induced damage, we briefly summarize below the relevant aspects of ion damage in solids. The process which is primarily responsible for inflicting damage to the matrix during the slowing down of energetic ions in a solid is nuclear collisions; i.e., close encounter Coulombic interactions which dislodge atoms. The process is statistical in nature and is well reproduced by TRIM,[23] a computer code which is based on Monte Carlo simulations. The TRIM code follows the trajectory of each impinging ion and of the target atoms displaced as a result of high momentum transfer collisions. Figures 3(A) and 3(B) show typical cascades resulting from the passage of a single 100 keV C ion and a single 320 keV Xe ion, respectively, slowing down in diamond. Statistics on many such randomly selected ion trajectories yields average values for the ion range and for the distribution of the various kinds of defects. It is important to stress that TRIM does not take into account dynamic annealing, defect diffusion, or the effects of the gradual accumulation of damage. Thus while TRIM can be successfully used to predict ion range and depth distributions of defects, care must be taken in extracting absolute defect concentrations from it. Indeed

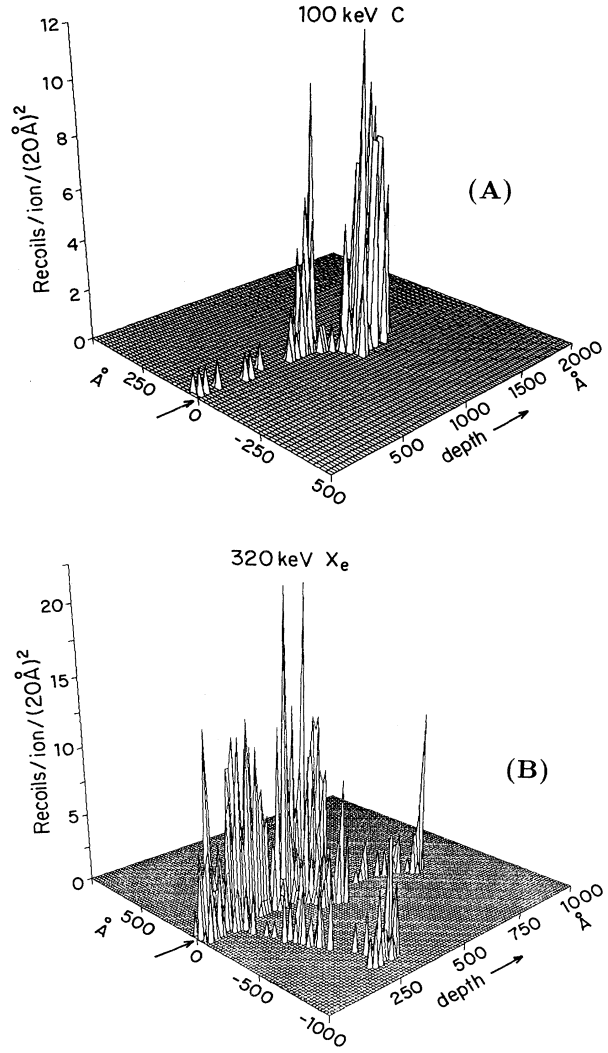

FIG. 3. Collision cascade following the penetration into diamond of (A) a single 100 keV C ion; and (B) a single 320 keV Xe ion, as calculated by the Monte Carlo computer code TRIM (Ref. 23).

TRIM almost always overestimates the defect concentration; with the best agreement expected for low-temperature implantations where most diffusion processes are suppressed. From Fig. 3 it is evident that the passage of each ion through the solid leaves a track of damage surrounding its trajectory. Along this track clusters of displaced atoms appear whenever high recoil energies have been given to host atoms. Hence, a good approximation of the damage around each ion track would be a distribution of damaged spheres of different radii. A more crude approximation which takes into account the average over many ions assumes the ion track to be surrounded by homogeneously distributed damage which is cylindrical in shape. Assuming that a cylinder of damage surrounds each ion track, TRIM can be modified to provide an estimate of the concentration of defects as a function of distance from the primary ion track at any given depth from the surface.[26] From such distributions, covering the entire region from the surface to the end of range of the ion, a root-mean-squared average radius r_{av} defined as

$$r_{av}=[\Sigma\rho_i r_i^2/\Sigma\rho_i]^{1/2} \tag{2}$$

can be calculated at any depth. Here ρ_i is the density of vacancies or interstitials created at a distance r_i from the ion track. The results of the average radius versus depth for both vacancies and interstitials are shown in Fig. 4 for

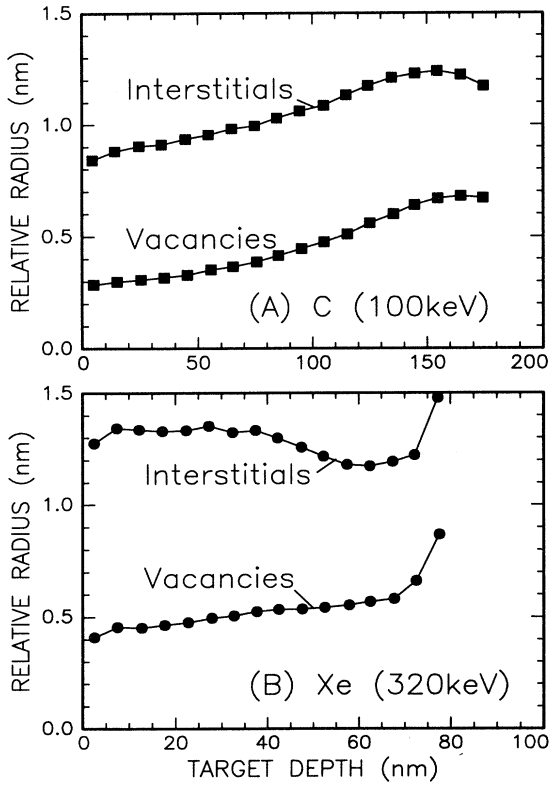

FIG. 4. The average radius of the damage cascade surrounding each ion track as a function of depth below the surface for (A) 100 keV C irradiation; and (B) 320 keV Xe irradiation as calculated by TRIM. The radius at each depth is estimated from the calculated distributions according to Eq. (2) (see text).

the irradiations with 100 keV C [Fig. 4(A) and 320 keV Xe [Fig. 4(B)]. In the absence of defect mobility, ballistic considerations dictate that vacancies will be more concentrated towards the center of the cascade whereas interstitials will tend to be concentrated further out from the center. Figure 4 reflects this, with a larger average radius for interstitials than for vacancies.

For the particular case of diamond, the damage centers (whether vacancies, interstitials, dangling bonds or defect clusters) can, in principle, act as electrically conducting sites. At low temperatures, where the damage is "frozen in" and bond rearrangement is unlikely, the simple picture provided above is probably adequate. However, at sufficiently high temperatures vacancies and interstitials can diffuse and either annihilate, disappear at the surface or agglomerate. Local bond rearrangement is also likely to occur. For the particular case of diamond, the agglomeration of defects and bond rearrangements may either result in graphitic or amorphous (sp^2 or sp^3 bonded) zones. The experimentally observed conductivity will thus depend on both the nature of the conducting centers and on their connectivity. For isolated conducting centers the electrical conductivity has been shown to be governed by hopping,[19,25] while for the case of graphitic islands when at such a concentration that connectivity is reached, metallic conduction typical of graphite is observed.[19]

The data of the present work as summarized in Fig. 1 can be understood in light of the above, i.e., (i) the differences in defect densities and distributions between those due to a heavy (Xe) and a light (C) implant and (ii) the ability of the defects to either annihilate or to form centers of different conductivities, as determined by the implantation temperature. Examination of Fig. 1 reveals that the functional dependence of R on dose is remarkably similar for Xe and C implants for the same implantation temperature, with the only difference being that the curves for C are displaced in dose by a factor of about 20 as compared to Xe. For the 690 K implants the similarity is not as obvious, mainly because the dose for the C implantations did not reach the high values required to observe the final drop in the resistivity evident for the Xe case.

The scaling of the R vs D curves for the Xe and C cases can be explained in terms of the average nuclear energy deposited by the ion beam in the irradiated volume. For a given ion species and energy, TRIM (Ref. 23) provides the fraction of energy lost by nuclear collisions (n) as well as the length of the track along which this loss occurs. The energy density (Q) deposited per ion in nuclear collisions is given by

$$Q=nE/[(R_p+\Delta R_p)\times 1.76\times 10^{23}]\ \text{eV/ion/cm}^3\ , \tag{3}$$

where E is the ion energy in eV, R_p and ΔR_p are the range and straggling, respectively, of the incident ion and 1.76×10^{23} atoms/cm^3 is the atomic density of diamond. By substituting into Eq. (3) values for n, R_p and ΔR_p as calculated by TRIM (Ref. 23) we obtain

$$Q_{Xe}/Q_C=17.5\ . \tag{4}$$

This means that the passage of a 320 keV Xe ion deposits on average 17.5 times more energy in the irradiated volume by nuclear processes than does the passage of a 100 keV C ion. Therefore the density of defects in a given volume is predicted to also be 17.5 times greater for the same number of impinging Xe ions than for C ions. Hence the above approach predicts that in order to achieve the same density of defects, and thus the same effect on the electrical conductivity, a dose 17.5 times higher for C than for Xe will be required. Indeed this factor calculated on the basis of TRIM is in good agreement with the experimental factor of 20 estimated above from the scaling of the data, thus proving that it is indeed the volume density of defects introduced by the ion which is responsible for the ion-beam-induced conductivity in diamond, irrespective of the ion species. It is important to note that the same scaling factor holds for all implantation temperatures employed.

We now turn to a possible microscopic model to explain the ion-beam-induced conductivity in diamond and its dependence on temperature. We assume that the passage of each ion through the solid leaves in its wake a "trail" of damaged spheres of average radius r (see Fig. 3). When the density of these spheres reaches a sufficient concentration, a connective pathway may be formed between them giving rise to a sharp decrease in the measured resistivity as is observed in the data at D_c (see Fig. 1). Following the approach of Ref. 17 the critical dose D_c should be related to r by

$$r=[(0.135\times(R_p+\Delta R_p)]/D_c)^{1/3} . \quad (5)$$

Hence, by knowing D_c, average radii of the spheres can be calculated. The doses D_c used to calculate r are indicated by arrows in Fig. 1 for all implantation temperatures employed and for both Xe and C implantations. (For the C implantation at $T_i=690$ K, D_c has been estimated to be 1.3×10^{17} C/cm^2 based on scaling the data for the Xe implantation). In Fig. 5, radii r extracted from the data by the use of Eq. (5) for Xe and C implantations are plotted as a function of implantation temperature. The fact that D_c is somewhat uncertain for the 150 K Xe implantation is reflected in the large error bar in the deduced value of r. Clearly r diminishes with increasing temperature, signifying the shrinkage of the conducting regions due to dynamic annealing (i.e., annealing during the passage of the ion through the solid).

Morehead and Crowder[27] have proposed a model for the formation of amorphous silicon under ion bombardment which may be applied to the present results. The model proposes that as the ion passes through the solid the thermal spike (lasting about 10^{-12} s) surrounding the ion track leaves in its wake highly disordered regions with many broken bonds. Morehead and Crowder[27] developed the theory for cylindrically shaped damaged regions around each ion track, but also considered spheres of damages which is the approach we will follow here. The damaged regions are assumed to be spheres of radius r_0. After the passage of the ion, the displaced atoms are assumed to relax to form a stable phase in a time $\tau\simeq10^{-9}$ s. During this time τ vacancies and interstitials can recombine in an outer sheath of thickness δr surrounding the ion core, leaving a stable amorphous sphere of radius $(r_0-\delta r)$. The magnitude of δr depends primarily on the implantation temperature. At low temperatures, when the diffusion of defects is inhibited, $\delta r=0$, and the radius of the sphere is as determined by ballistic considerations. The model also predicts the existence of a temperature T_∞ for which $\delta r=r_0$, i.e., the whole of the sphere is annealed and no amorphous zone is created. Experimentally, this is the implantation temperature at or above which Si cannot be amorphized no matter how high the dose.

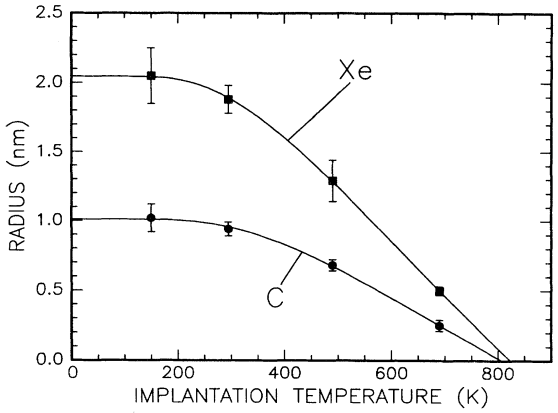

FIG. 5. The radius of the damage spheres as a function of implantation temperature for 100 keV C and 320 keV Xe irradiations. The solid lines are fits of the data to the equation $r(T)=r_0[1-B\exp(-U/k_BT)]$ with $r_0=1.01$ nm, $U=0.12$ eV, and $B=5.40$ for 100 keV C implantations and $r_0=2.04$ nm, $U=0.10$ eV, and $B=4.24$ for 320 keV Xe irradiations. Extrapolation of the fits for both Xe and C implantations to high temperatures predicts that the radius of the damage spheres should shrink to zero for an implantation temperature of about 815 K. Extrapolation to low temperatures predicts that the radius of the damage spheres at 0 K should be 1.01 and 2.04 nm for C and Xe implantations, respectively.

If we replace the amorphous spheres considered in Ref. 27 by conducting spheres of graphitelike material, the Morehead and Crowder model can be directly applied to the present data. The model predicts that the radius of the conducting sphere as a function of implantation temperature should be given by

$$r(T)=r_0[1-B\exp(-U/k_BT)] , \quad (6)$$

where r_0 is the radius of the conducting sphere in the absence of defect diffusion (i.e., for $T_i=0$ K), $U=E_{df}/2$ where E_{df} is the activation energy for defect diffusion, k_B is Boltzman's constant and B is a constant which depends on the stopping power of the incident ion, the diffusion time τ, the number of target atoms/cm^3, and the displacement energy.

The solid lines in Fig. 5 are least-squares fits of the data to Eq. 6 obtained by varying the parameters r_0, U, and B. For 100 keV C implantations the fitted values of r_0, U, and B are 1.01 nm, 0.12 eV, and 5.40, respectively, while

the respective values for the 320 keV Xe implantations are 2.04 nm, 0.10 eV and 4.24. Although the number of data points is small, it is clear that Eq. (6) does provide an excellent description of the functional form of $r(T)$. In particular, the fits for both the Xe and C implantations provide an estimate for the activation energy for defect diffusion of about 0.2 eV. This value is small as compared to the measured activation energy for C interstitial diffusion in diamond of 1.3 eV.[28] However, most previous work has measured the activation energy for post-irradiation annealing, whereas E_{df} is a measure of the activation energy for diffusion during the thermal spike. Thus, the reason for the low value of E_{df} obtained here must be the well-known phenomenon of radiation-enhanced diffusion. For example,[29] for the case of C interstitial diffusion in ion-irradiated glassy carbon, the activation energy for post-implantation annealing was measured to be 0.6 eV, whereas a value of only 0.1 eV for the activation energy was obtained in this material for dynamic annealing during the implantation.

The extrapolation of the fits to the data yields for the zero radius intercept an implantation temperature of 804 K for C and 820 K for Xe implantations, respectively, i.e., at an implantation temperature of about 815 K the damage introduced by the passage of the ions is annealed during the time τ so that no identifiable damage region is left behind. This estimate of 815 K as the temperature at which the radius of the damage track shrinks to zero is in reasonable agreement with the temperature at which the swelling which accompanies ion beam irradiation was found to diminish to zero.[21] A temperature of about 800 K is also the temperature at which vacancies are thought to become mobile (interstitials being mobile already at around 300 K).[8] It is therefore reasonable to conclude that for $T_i > 815$ K instantaneous recombination of interstitial-vacancy pairs or their disappearance by some other diffusive process occurs, thus inhibiting the formation of stable defects. Based on the above, the temperature of 815 K should also be the minimum temperature at which high dose implantation into diamond will not result in graphitization or amorphization. For the special case of high dose C implantation into diamond, this should be the minimum temperature at which diamond growth can be expected. Indeed it has been shown by Freeman, Temple, and Guard[30] and Nelson *et al.*[31] that heavy dose carbon ion implantation into diamond held at high temperature results in diamond growth.

As mentioned above TRIM should be most applicable for low-temperature implantations where defect diffusion is minimized. Extrapolation of the radii of Fig. 5 to 0 K should give a value for the maximum average radius r_0 of the damage spheres when dynamic annealing effects are at a minimum. From the fits to the data in Fig. 5, these radii are found to be 2.04 nm for Xe and 1.01 nm for C implantations. These values should be compared with the radii obtained from the TRIM calculations shown in Fig. 4 which are about 1.4 nm for 320 keV Xe irradiations and vary from 0.9 nm at the surface to about 1.2 nm towards the end of range for 100 keV C irradiations. The agreement of the measured values of the radii with those calculated by TRIM is very satisfactory, especially when it is recalled that the TRIM calculations are based on a cylindrical model for the damage cascade, which is clearly an oversimplification. The measured values of r_0 are also in reasonable agreement with those measured for ion induced cascades in other materials.[32] In particular, a radius of about 2 nm is consistent with the size of the hillocks formed as a result of single ion impacts in highly oriented pyrolytic graphite.[33] In that case scanning tunneling microscopy (STM) revealed hillocks on the surface of average radius 2.3 nm for 50 keV Ar irradiation and 2.6 nm for 150 keV Xe irradiation. For diamond implanted with 120 MeV Kr ions,[34] STM revealed craters of average radius 1.5 nm, which is also consistent with the values obtained here, despite the much larger energy of the incident Kr ions as compared to the Xe and C ions used in the present work.

For the implantations performed at 150 K, for which negligible instantaneous annealing is expected, the measurements of the temperature dependence of the conductivity and the above deduced values for the size of the conducting spheres can be used to provide an estimate for the density of states at the Fermi level $N(E_F)$ for heavily irradiated diamond. By using the values of T_0 obtained from the plots in Fig. 2, and the relationship

$$N(E_F)=16\lambda^{-3}/k_B T_0 , \tag{7}$$

where k_B is Boltzmann's constant and λ is the radius of the localized wave function, $N(E_F)$ can be calculated.[24] By assuming that each conducting sphere serves as one center for hopping conduction so that $\lambda \simeq$ the radius of the conducting spheres as determined by Eq. (5), one obtains $N(E_F) \simeq 2\times 10^{19}$ states/eV/cm^3 for diamond irradiated with 2×10^{16} Xe/cm^2 and $N(E_F) \simeq 4\times 10^{18}$ states/eV/cm^3 for irradiation with 8×10^{16} C/cm^2. These values are low by comparison with the atomic density of diamond, but are quite consistent with the results of obtained by Hauser *et al.*[19] In Ref. 19 this low concentration of conducting centers was used to explain why diamond can retain most of its hardness despite very large increases in its conductivity, since only a small percentage of diamond bonds are converted into sp^2 conducting sites even in heavily damaged diamond. These considerations raise the question how many conducting centers are created per incident C or Xe ion; a question which will be addressed below.

It should be noted that the sharpness of the drop at D_c is the greatest for 490 K implantations and in particular that it is sharper than for 295 K implantations. Data of $R(D)$ for 320 keV Sb implanted into diamond at room temperature (which are very similar to the 300 K Xe implantation data shown here) have been analyzed in Ref. 17 using a percolation approach. Assuming a simple model of percolation between highly conducting spheres dispersed in an insulating matrix one would expect the resistance to vary with dose as[17]

$$R=R_s\times[1-(2/3)^{(D/D_c)-1}]^{-1} , \tag{8}$$

where R_s is the saturation resistance at high doses (which in this model is the resistance of the individual conducting spheres) and D_c is the critical dose for the onset of the

conductivity. For $D < D_c$, the spheres do not percolate so $R = \infty$.

In Fig. 6, the resistance of the diamond is plotted as a function of ion dose close to D_c for Xe implantation at 295 and at 490 K, together with the theoretical prediction according to Eq. (8). The simple theory employed in Ref. 17 assumes percolation between spheres with sharply defined boundaries, i.e., being highly conducting inside the sphere and nonconducting outside. Indeed, from the agreement between the data for 490 K Xe implantation and the behavior predicted by Eq. (8) [Fig. 6(B)], the situation for the 490 K implantations approaches this condition.

However, as was found in Ref. 17, for the implantation at 295 K, Eq. (8) predicts a decease in R at D_c which is much sharper than that actually observed. For implantations below room temperature, it is likely that the boundaries of the damage spheres are less well defined being more conducting in the center and less towards the edges where the defect density tapers off. Such a tapering is reasonable in view of the fact that ballistic considerations dictate that the "core" of the sphere should be rich in vacancies whereas the periphery would be expected to be rich in interstitials,[35] as is indeed borne out by the TRIM calculations shown in Fig. 4. For room-temperature implantations vacancies are almost completely immobile, while interstitials are able to diffuse at least to some degree.[8] In this case, one may expect a high concentration of vacancies at the center of the damage sphere, with an interstitial concentration being more spread out towards the periphery of the sphere. As a consequence, the percolative transition should be more gradual than that predicted by a simple "conducting/insulating" theory. On the other hand, for elevated temperature implantations (> 470 K) point-defect diffusion is possible, resulting in both a shrinkage of the size of the conducting centers and in the sharpening of their boundaries. The shrinkage of the spheres with increasing T_i is experimentally verified by the data and fits shown in Fig. 5, while the proposition that the spheres sharpen for elevated T_i finds support in the sharpness of the $R(D)$ drop around the critical dose D_c.

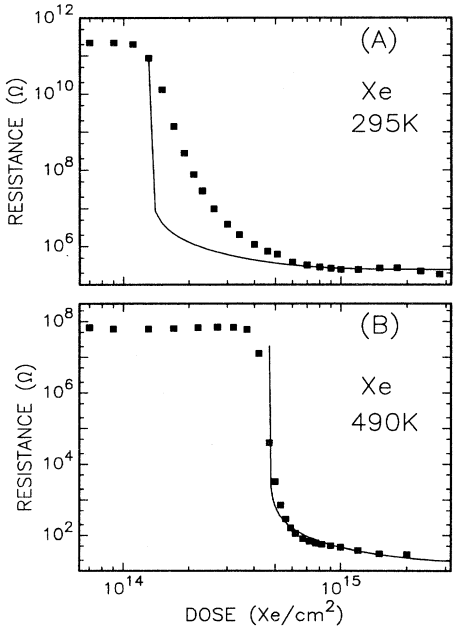

FIG. 6. Resistance of diamond as a function of ion dose for 320 keV Xe implantations performed at 295 K (A) and 490 K (B). The solid line is the theoretically expected dependence described by Eq. (8) assuming a simple model of percolation between conducting spheres. It is clear that for implantation at 295 K the transition is too gradual to be accounted for by this simple model. However, for implantation at 490 K the dose dependence of the resistance is close to that expected by a simple percolative transition.

We now turn to discuss the variation of the high dose saturation resistivities R_s as a function of implantation temperatures. Very low saturation values are found for the case of 470 K implantations for both C and Xe and for Xe implanted diamond at 690 K. However, in light of the scaling between Xe and C described above, low saturation values will almost certainly be reached also for the 690 K C implantations at doses, however, higher than those employed here. These saturation values are close to the resistivity of graphite and reflect the high internal conductivity of each one of the conducting spheres. As the implantation temperature is increased the damage spheres, which have a tapered density of defects for low implantation temperatures, partially anneal and partially graphitize, thus contracting to spheres of smaller radii with graphitic conductivity. This trend does not continue indefinitely because, as indicated above, complete instantaneous annealing inhibits the formation of conducting spheres at implantation temperatures in excess of about 815 K. Above this temperature ion-beam irradiation leaves the implanted material highly insulating at any dose, the material being predominantly diamond, however containing a high number of extended defects, in accord with the findings of Refs. 31 and 36.

At low implantation temperatures the minimum resistivities even at high doses are rather high. In this case overlap of the damage spheres does occur at sufficiently high doses but the internal conductivity of the damage spheres themselves is not as high as it is in the case of the high temperature implantations. Data of the resistivity of diamond implanted to a given (fixed) high dose as a function of implantation temperature have been unpublished by Sato and Iwaki[12] and Prins.[8] In the case of Ref. 8 a minimum in R_s is reported to occur for C implantations at about 500 K for a C dose of about 1×10^{17}C/cm^2, and that for implantations at higher temperatures, R_s rises due to the effects of dynamic annealing. The assumption is that this dose is sufficient to see the saturation of the resistivity. However, the data of the present work (see Fig. 1) shows that if higher doses or heavier ions are employed, the same final very low R_s can be obtained for both 490 and 690 K implantations. The value of R_s in these cases is comparable to that expected from polycrystalline graphite, thus suggesting that for implantation temperatures exceeding about 470 K, the conducting spheres are graphitic in nature.

In the dose range below D_c, a peculiar nonmonotonic behavior is observed (see Fig. 1) which is particularly

striking for 300 K C implantations, but is also evident for higher implantation temperatures. For 300 K implantations a minimum is recorded at dose D_1 (see Fig. 1). For implantations at 470 K this minimum becomes very shallow approaching a plateau and it moves up in dose. Such a minimum is not noticeable for the cold implantations; however we speculate that it may have been observed were it not for the limitations of the measurements of the high resistances involved. For implantations at 690 K the functional form of R vs D is even more complicated displaying multiple plateaus not previously observed.

The material transformations which lead to this peculiar behavior of the $R(D)$ data are difficult to explain. However it should be noted that EPR measurements on diamond implanted with 350 keV Sb ions at room temperature[10] have also shown nonmonotonic trends exhibiting a local maximum in the EPR signal and linewidth at a dose close to D_1.

We begin our discussion of this dose regime with reference to the implantations at 490 K, for which it is clear [see Fig. 6(B)] that a simple model of percolation between conducting spheres holds reasonably well. At doses well below D_c, one may expect that nearest-neighbor hopping should occur between these conducting spheres. For nearest-neighbor hopping conduction the resistance R is primarily governed by the tunneling probability between a pair of states separated by a typical distance of the order of $N^{-1/3}$, which is the average distance between hopping centers whose volume concentration is N. The expected functional dependence[17] is

$$R \propto \exp(\gamma N^{-1/3}\lambda^{-1}) , \tag{9}$$

where γ is a numerical coefficient of the order of unity, and the parameter λ is the characteristic dimension of a localized state on a hopping center. For conducting centers introduced by ion implantation, N would be expected to be proportional to the ion dose D (in ions/cm^2) at least for low doses, i.e.,

$$N=\beta\times D/W , \tag{10}$$

where $W=R_p\pm\Delta R_p$ is the thickness of the implanted region (in cm) and β is a numerical factor equal to the number of hopping centers created by each incident ion. By combining Eqs. (9) and (10) it is evident that for hopping conduction a plot of $\log(R)$ vs $D^{-1/3}$ should yield a straight line.

In Fig. 7, the portion of the data of Fig. 1 for $D<D_c$ are plotted as $\log_{10}(R)$ vs $D^{-1/3}$ for 100 keV/C implantations at 470 K. In Fig. 8 a similar plot is provided for 320 keV Xe implantations at 490 K. From the plots it is clear that the hopping picture as described by Eq. (9) well describes both the Xe and C data over about a decade of dose in the dose regime well below D_c. However, as was pointed out in Ref. 17 the simple hopping model described by Eq. (9) is expected to break down at high enough concentrations where variable range hopping takes over.

We now estimate the number of conducting centers created by each impinging C or Xe ion. If one makes the reasonable assumption that λ in Eq. (9) (which is the characteristic dimension of the localized hopping center) is equal to the radius of the conducting spheres, λ can be estimated from Fig. 5 to be 0.7 and 1.3 nm for C and Xe implantations, respectively, at 490 K. From Eqs. (9) and (10) the number of conducting spheres created per incident ion β should be given at

$$\beta\simeq W\times(S\lambda)^{-3} , \tag{11}$$

where S is the slope of the fit to the $\ln(R)$ vs $D^{-1/3}$ curves, and where we have assumed $\gamma\simeq 1$.

By extracting the slope S from Figs. 7 and 8, and by using $W=150$ and 65 nm for C and Xe implantations, respectively, we obtain $\beta(\mathrm{C})\simeq 0.6$ and $\beta(\mathrm{Xe})=0.9$. Thus, according to this analysis, the number of conducting spheres created per incident ion is extremely low. This is a remarkable result since one may have expected many knock on carbon interstitial and vacancies to be created in the collision cascade as the impinging ions passes through the solid. For example, TRIM (Ref. 23) predicts that about 100 carbon vacancies are created per incident 100 keV C ion, whereas about 1000 such vacancies are created for each impinging Xe ion. However, it must be borne in mind that these vacancies and interstitials may

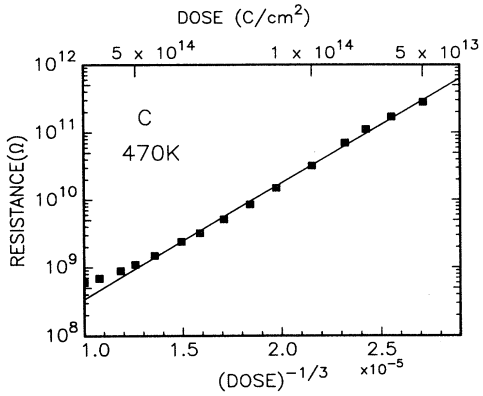

FIG. 7. The resistance of diamond as a function of dose for implantation with 100 keV C ions at 470 K (see Fig. 1), replotted as $\log_{10}(R)$ vs $D^{-1/3}$.

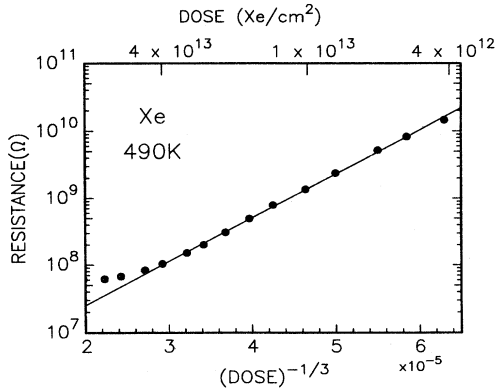

FIG. 8. The resistance of diamond as a function of dose for implantation with 320 keV Xe ions at 490 K (see Fig. 1), replotted as $\log_{10}(R)$ vs $D^{-1/3}$.

cluster and hence the number of clusters will be less than the number of vacancies. In addition, as pointed out above, TRIM does not take into account dynamic annealing. Clearly for the case of the 490 K implantations such annealing is very important, leaving, as deduced from the above discussion, only one conducting center on average per incident ion. At first glance it may also appear strange that the Xe ion does not create a greater number of spheres per incident ion than for C implantations, given that D_c for Xe is about a factor of 20 less than for C implantations. However, a closer investigation reveals that the factor of 20 can be accounted for by the fact that the spheres created by the Xe implantation are on average about twice the radius of the spheres created by the C implantation and thus 8 times the volume. In addition these spheres are confined to a thickness of about 65 nm as compared to a thickness of about 150 nm for the C implantations. Thus, despite the fact that on average only about one sphere is created per incident ion for both C and Xe irradiations, the spheres touch and percolation occurs at a much lower dose for Xe than for C implantations because (i) the spheres are larger and (ii) the spheres are concentrated in a smaller volume.

The above approach assumes a unique radius for the damage spheres (which is a function of implantation temperature and ion species). Clearly this is an oversimplification as one might expect a distribution of sizes of the damage spheres around each ion track due to the statistical nature of the collision cascade. Indeed this is found to be the case in the TRIM calculations, the results shown in Figs. 3 and 4 being the average of the calculations for many collision cascades. The onset of hopping and percolation depend, in principal, on the volume of transformed material and this volume is heavily dominated by the largest spheres which are created in the collision cascade. Thus, the conclusion that there is only about one sphere created per incident ion strictly relates to spheres of the largest radius, and does not take into account the possibility that spheres of smaller radius may also be created at the same time. The analysis used above cannot determine the distribution of sphere radii; for this TEM and/or atomic force microscopy investigations are required. However, it is clear that the percolation and hopping will be dominated by the largest sized spheres, and this serves as a justification for neglecting the possible contribution of smaller spheres to the phase transformation.

The situation for implantation at 150 and 295, and 690 K is more complicated, and cannot be explained by recourse to the very simple model proposed above. Firstly, the changes in R vs D are not sufficiently sharp to be explained by simple percolation; therefore one is forced to conclude that the spheres are not spatially well defined and may well be "graded" in their conductivity. Secondly, Eqs. (9) and (10) do not well describe the data for implantation at 150 and 295 K, although the data for the 690 K implantations for low doses can be analyzed in a similar fashion to the 490 K data and with a similar result; viz., the number of conducting centers per incident ion is of the order of unity. Thirdly, the data for 295 K implantations shows nonmonotonic behavior which is not compatible with the simple hopping/percolation model proposed above.

It is clear that a minimum such as that observed in the R vs D data most clearly for 295 K implantations at D_1 (see Fig. 1) must be the result of two opposing processes; one leading to an increase in electrical conductivity with increasing dose and another to its decrease with the observed conductivity being the net result of these two competing processes. As mentioned previously, nonmonotonic behavior is also observed in the ESR measurements[10] which show a local maximum in the spin density and linewidth at D_1. We note that this very unusual nonmonotonic behavior appears to be unique to diamond and diamonds films[18] and does not occur for other forms of carbon. At present the processes responsible for this behavior remain unclear and are under further investigation.

In closing we wish to point out an interesting observation regarding the comparison of the present data to the results of similar measurements on C implanted fused quartz.[25] The above discussion on the defect-induced conductivity in diamond was based on the notion that conducting centers created by the damage cascade embedded in a matrix of insulating diamond are responsible for the observed conductivity. In principle, this system may be analogous to the case in which C atoms are implanted into an insulating medium such as SiO_2, provided that it can be established that the conductivity in the insulator is due the presence of the C atoms and not to ion-beam-induced damage. This is the case for 100 keV C implantation into fused quartz[25] for which it has been shown for both room temperature and 470 K implantations that the conductivity depends only on the presence of the implanted C atoms in the matrix and not on the ion beam damage. It is therefore reasonable to try and compare the R vs D data for C implanted fused quartz and damaged diamond, since in both cases it is the presence of dislodged (in the case of diamond) or implanted (in the case of fused quartz) C atoms in an insulating matrix which gives rise to the observed conductivity.

In Fig. 9 the results of the change in resistivity with in-

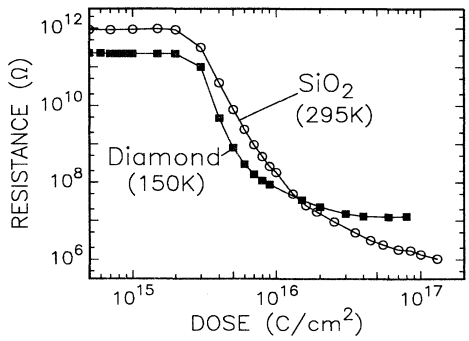

FIG. 9. Comparison of the dose dependence of diamond and fused quartz for 100 keV C implantation. The implantation temperatures are shown in the figure. Note that for low-temperature irradiations the dose dependence for fused quartz and diamond are very similar, and that the onset of conductivity occurs at the same critical dose.

creasing ion dose for room-temperature implantation of C into SiO_2 (from Ref. 25) are overlaid with the data for 150 K C implantation into diamond (from Fig. 1). The diamond and fused quartz resistivities shown are remarkably similar in both absolute values as well as in their functional dependence on C ion dose.[37] This is once again extraordinary in view of the fact that every C ion impinging onto diamond is expected to knock many hundreds of C atoms out from their lattice positions in the collision cascade, each potentially contributing to the conductivity. As this "multiplication" of liberated C atoms and their contribution to the conductivity does not occur in SiO_2 it is most unexpected that the same conductivity is generated for a given C ion dose in quartz as is obtained in diamond. However, the results are consistent with the observation of a low value for $N(E_F)=4\times10^{18}$ states/eV/cm^3 for these low-temperature C implantations into diamond for which presumably only a small fraction of the broken bonds are electrically active.

One possibility to account for the above observation would be the near complete annihilation of the vacancy interstitial pairs created by the damage cascade so that on average only one conducting center is created per incident C ion as we have shown to be the case for 490 K implantations. However, as discussed above, this simple picture does not hold for lower temperature implantations where defect mobilities are low. In this case we have shown that the conduction mechanism in damaged diamond is complicated and depends on the interplay between defects which may display different kinds of conductivity. Notwithstanding the above difficulties in interpretation, the similarity between the two cases shown in Fig. 9 is striking.

V. SUMMARY

The changes in electrical conductivity of diamond, damaged by either carbon or xenon ion implantation have been studied. In contrast to previous work which has addressed only selected regions in ion dose, or implantations at a single target temperature, the present work covers the complete range of ion doses over which changes in the resistance are observed from 1×10^{12} ions/cm^2 at which ion-beam-induced conductivity can first be observed, up to the highest dose (1×10^{17} ions/cm^2) at which saturation of the conductivity occurs.

By comparing the results of the electrical resistance as a function of dose $R(D)$ for Xe and C implantations and for a range of implantation temperatures from 150 up to 690 K, it was possible to propose a model for the ion-beam-induced transformation of diamond, based on a consideration of the damage produced around each ion track and the dependence of this damage on implantation temperature. The main points of this model are

(i) For low implantation temperatures, clusters of point defects are formed around each ion track, between which hopping conduction occurs.

(ii) At higher implantation temperatures, these clusters either disappear or shrink to a smaller average radius due to dynamic annealing. At low doses nearest-neighbor hopping occurs between these spheres, but at a critical dose, percolation occurs to form a conductive pathway with graphitelike conductivity. The dynamic annealing is very efficient with, on average, only one conducting sphere remaining for effective conduction per incident C or Xe ion.

(iii) The temperature dependence of the radius of the conducting spheres is well described by the Morehead and Crowder approach which assumes that annealing takes place in a sheath surrounding the damage sphere, and that the thickness of the sheath increases with increasing implantation temperature. The fit of this model to the data predicts the complete disappearance of the conducting spheres due to instantaneous annealing for implantation temperatures exceeding 815 K. Under these conditions, graphitization of the diamond will never occur regardless of the ion dose. The model also predicts an activation energy for defect (probably interstitial) diffusion during ion irradiation of about 0.2 eV.

(iv) For intermediate implantation temperatures, the low dose regime displays a minimum in the $R(D)$ curves. The origin of this nonmonotonic behavior is not known at present, although it may be due to a competition between two processes such as, for example, the production of p-type conductivity due to point defects competing with n-type conductivity which occurs when these defects agglomerate at higher doses. One other possibility, is that the competition may be between the contribution to the conductivity due to the presence of isolated point defects and the effective removal of electrically active states in the band gap when these points defects agglomerate into more complex defect structures at higher doses.

(v) The $R(D)$ data are remarkably similar for both Xe and C implantations, with the only difference being that the doses required to produce a given conductivity are a factor of 20 higher for C than Xe implantations. On a macroscopic level this factor is explained by the fact that the density of nuclear energy deposited per incident ion is about 20 times higher for Xe than C implantations, thus demonstrating that it is the density of collisionally induced defects which governs the electrical conductivity in ion-damaged diamond. On a microscopic level the factor of 20 can be explained by the fact that the volume of conducting spheres formed around each ion track is about eight times larger for Xe than C implantations and that these spheres are packed into a layer which is about half the thickness for Xe and C implantations due to the shorter range of the Xe as compared to the C ions used in the irradiations.

ACKNOWLEDGMENTS

S.P. would like to acknowledge the generous and ongoing hospitality of the Solid State Institute at the Technion where the experimental work reported in this paper was carried out. We are most grateful to Dr. Q. Yang of the Department of Physics, University of Newcastle for performing the modified TRIM calculations reported herein. This work was supported in part by the Department of Industry, Technology and Regional Development, and by the Australian Research Council for S.P. and by the European Economic Community (Contract No. 3019-1-89) for R.K.

[1]J. E. Field, *The Properties of Natural and Synthetic Diamond* (Academic, London, 1992).
[2]D. R. McKenzie, D. A. Muller, E. Kravtchinskaia, D. Segal, D. J. H. Crockayne, G. Amaratunga, and R. Silva, Thin Solid Films **206**, 198 (1991).
[3]V. S. Vavilov, V. V. Krasnopevtsev, Y. V. Milijutin, A. E. Gorodetsky, and A. P. Zakharov, Radiat. Eff. **22**, 141 (1974).
[4]B. Miller, R. Kalish, L. C. Feldman, A. Katz, N. Moriya, K. Short, and A. E. White, J. Electrochem. Soc. **141**, L41 (1994).
[5]J. F. Prins, Appl. Phys. Lett. **41**, 950 (1982).
[6]S. Prawer, A. D. Devir, L. S. Balfour, and R. Kalish, Appl. Opt. **34**, 636 (1995).
[7]M. S. Dresselhaus and R. Kalish, *Ion Implantation in Diamond, Graphite and Related Materials* (Springer-Verlag, Berlin, 1992).
[8]J. F. Prins, Mater. Sci. Rep. **7**, 271 (1992).
[9]G. Braunstein, A. Talmi, R. Kalish, T. Bernstein, and R. Besserman, Radiat. Eff. **48**, 139 (1980).
[10]M. Teicher and R. Besserman, J. Appl. Phys. **53**, 1467 (1982).
[11]S. Connell, J. D. Comins, and J. P. F. Sellschop, Radiat. Eff. Exp. **2**, 57 (1988).
[12]S. Sato and M. Iwaki, Nucl. Instrum. Methods Phys. Res. Sect. B **32**, 145 (1988).
[13]J. F. Prins, Radiat. Eff. Lett. **76**, 79 (1983).
[14]F. Fang, C. A. Hewett, M. G. Fernandes, and S. S. Lau, IEEE Trans. Electron. Devices **36**, 1783 (1989).
[15]C. Uzan-Saguy, V. Richter, S. Prawer, Y. Lifshitz, E. Grossman, and R. Kalish, Diamond Relat. Mater. (to be published).
[16]A. Hoffman, S. Prawer, and R. Kalish, Phys. Rev. B **45**, 12 736 (1992).
[17]R. Kalish, T. Bernstein, B. Shapiro, and A. Talmi, Radiat. Eff. **52**, 153 (1980).
[18]S. Prawer, A. Hoffman, and R. Kalish, Appl. Phys. Lett. **57**, 2187 (1990).
[19]J. J. Hauser J. R. Patel, and J. N. Rodgers, Appl. Phys. Lett. **30**, 129 (1977).
[20]J. F. Prins, T. E. Derry, and J. P. F. Sellschop, Phys. Rev. B **34**, 8870 (1986).
[21]R. A. Spits, T. E. Derry, J. F. Prins, and J. P. F. Sellschop, Nucl. Instrum. Methods. Phys. Res. Sect. B **51**, 63 (1990).
[22]S. Prawer, R. Kalish, M. E. Adel, and V. Richter, J. Appl. Phys. **61**, 4492 (1987).
[23]J. Zeigler, J. P. Biersack, and U. Littmark, *The Stopping and Range of Ions in Solids* (Pergamon, New York, 1985).
[24]N. F. Mott and E. A. Davis, *Electronic Processes in Noncrystalline Solids* (Clarendon, Oxford, 1979).
[25]S. Prawer, A. Hoffman, M. Petravic, and R. Kalish, J. Appl. Phys. **73**, 3841 (1993).
[26]Q. Yang (unpublished).
[27]F. F. Morehead, Jr. and B. L. Crowder, Radiat. Eff. **6**, 27 (1970).
[28]B. Massarini and J. C. Bourgoin, Phys. Rev. B **14**, 3682 (1976).
[29]D. G. McCulloch and S. Prawer, J. Appl. Phys. (to be published).
[30]H. Freeman, W. Temple, and G. A. Guard, Nature (London) **275**, 634 (1978).
[31]R. S. Nelson, J. A. Hudson, D. J. Mazey, and R. C. Piller, Proc. R. Soc. London, Ser. A **386**, 211 (1983).
[32]R. Kalish, L. C. Feldman, D. C. Jacobson, B. E. Weiss, J. L. Merz, L. Y. Kramer, K. Doughty, S. Stone, and K. K. Law, Nucl. Instrum. Methods. Phys. Res. Sect. B **80/81**, 729 (1993).
[33]L. Porte, M. Phaner, C. H. de Villeneuve, N. Moncoffre, and T. Tousset, Nucl. Instrum. Methods Phys. Res. Sect. B **44**, 116 (1989).
[34]V. S. Varichenko, A. M. Zaitsev, M. S. Rusetskii, V. F. Stelmakh, K. de Weldige, Th. Freis, K. Wandelt, A. Ju. Didyk, and V. A. Laptev, Diamond Related Mater. **3**, 711 (1994).
[35]I. H. Wilson, N. J. Zheng, U. Knipping, and I. S. T. Tsong, Phys. Rev. **38**, 8444 (1988).
[36]G. Braunstein and R. Kalish, Nucl. Instrum. Methods Phys. Res. **209/210**, 387 (1983).
[37]For a precise comparison between the two cases, it would be necessary to compare resistivities, rather than the measured resistances. Conversion from resistance to resistivity involves taking into account the contact geometry and the range of the ions in each case. As the experiments were performed under very similar conditions and with similar contact geometries for both C implantation of fused quartz and C implantation of diamond, the differences in the conversion factors for the two cases were estimated to be no more than a factor of 2 at most, and hence do not alter the conculsions reached here.